scientific reports

Check for updates

OPEN

Evaluating facial dermis aging in healthy Caucasian females with LC-OCT and deep learning

Ali Assi[1], Sébastien Fischman[2], Colombe Lopez[2], Mélanie Pedrazzani[2], Guénolé Grignon[1], Raoul Missodey[1], Rodolphe Korichi[1], Jean-Hubert Cauchard[1], Samuel Ralambondrainy[1] & Franck Bonnier[1]✉

Recent advancements in high-resolution imaging have significantly improved our understanding of microstructural changes in the skin and their relationship to the aging process. Line Field Confocal Optical Coherence Tomography (LC-OCT) provides detailed 3D insights into various skin layers, including the papillary dermis and its fibrous network. In this study, a deep learning model utilizing a 3D ResNet-18 network was trained to predict chronological age from LC-OCT images of 100 healthy Caucasian female volunteers, aged 20 to 70 years. The AI-based protocol focused on regions of interest delineated between the segmented dermal-epidermal junction and the superficial dermis, exploiting complex patterns within the collagen network for age prediction. The model achieved a mean absolute error of 4.2 years and exhibited a Pearson correlation coefficient of 0.937 with actual ages. Furthermore, there was a notable correlation ($r = 0.87$) between quantified clinical scoring, encompassing parameters such as firmness, elasticity, density, and wrinkle appearance, and the ages predicted by deep learning model. This strong correlation underscores how integrating emerging imaging technologies with deep learning can accelerate aging research and deepen our understanding of how alterations in skin microstructure are related to visible signs of aging.

Keywords Skin aging, Collagen network, Age estimation by deep learning, Artificial Intelligence, Line field confocal optical coherence tomography (LC-OCT), Non-invasive imaging

Skin aging is a multifaceted biological phenomenon encompassing both chronological (intrinsic) aging, which occurs naturally with time, and photoaging (extrinsic aging), driven primarily by external factors such as ultraviolet (UV) radiation exposure. Extrinsic aging is further influenced by various environmental factors, including pollution as well as lifestyle habits such as smoking, poor diet, and sleep deprivation. The aging process, particularly in the context of facial aging, holds significant societal implications. It shapes individual perceptions of age and contributes to the development of skin disorders associated with advanced aging processes. Comprehending the mechanisms and consequences of skin aging lays the groundwork for innovative treatments, enhanced skincare practices, and improved quality of life for individuals across all age groups. Hence, it has become a major field of innovation within the dermatology community and beauty industry, underscored by significant evolution in assessment tools and methods[1].

At the macroscopic level, aging manifestations are often evaluated using clinical scoring systems and atlases devised by researchers and dermatologists. These indicators encompass a spectrum of visible changes, including wrinkles, fine lines, sagging, uneven pigmentation, and diminished elasticity[2]. One widely employed tool for assessing skin aging is the Bazin atlas, which provides a standardized framework for evaluating various aspects of aging through visual and tactile examinations[3]. Over the years, numerous scoring systems have been reported in the literature, offering quantitative measurements of facial aging. These allow for objective comparisons between individuals and tracking changes over time. Examples include the SCINEXA (Skin Aging INEXplicit Assessment) score, which was developed as a comprehensive tool for standardized and quantitative evaluation of facial aging. It is based on five items characteristic of intrinsic skin aging and includes eighteen items related to extrinsic skin aging[4]. Another example is the Fitzpatrick Scale, primarily used to assess skin type and susceptibility to sunburn but also indicative of aging-related changes in skin pigmentation[5].

At the microscopic level, researchers have long focused on providing in vivo instrumental assessments to characterize modifications occurring within sub-skin surface microstructure through non-invasive

[1]LVMH Recherche, 185 Avenue de Verdun, 45800 Saint Jean de Braye, France. [2]DAMAE Medical, 14 Rue Sthrau, 75013 Paris, France. ✉email: fbonnier@research.lvmh-pc.com

characterization of histological and cellular features. Various imaging techniques, such as Reflectance Confocal Microscopy (RCM) and Confocal Laser Scanning Microscopy (CLSM), have emerged as valuable tools, enabling the visualization of epidermal and superficial dermal layers at cellular resolution[6]. Multiphoton microscopy (MPM), another powerful imaging modality, utilizes near-infrared light to excite fluorescent molecules within the skin, allowing for non-destructive imaging of deeper skin layers. This technique provides valuable information about collagen fibrous organisation, elastin content, and skin hydration. Moreover, the integration of Multiphoton Microscopy (MPM) with cutting-edge imaging technologies such as second harmonic generation (SHG)[7] microscopy has significantly advanced the ability to visualize skin microstructures in unprecedented detail. These techniques not only provide high-resolution images but also offer quantitative biomarkers, or metrics, related to cellular morphology, density, and arrangement. Additionally, they facilitate the assessment of collagen and elastin organization, which are crucial indicators of skin health and aging[8]. Computer vision algorithms, fuelled by artificial intelligence (AI) and supplemented by other mathematical methodologies, have enabled correlations to be identified between specific quantitative parameters and age-related alterations in skin characteristics through machine learning techniques. These models also enable the creation of scoring indices to quantify aging effects. For instance, the SAAID (SHG to Autofluorescence Aging Index of Dermis) offers a numeric depiction of the aging condition of the dermal layer, as observed through multiphoton microscopy[9]. Alternative scoring indices have also been proposed. The MLT-based Dermis Morphology Score (MDMS), for instance, utilises multiphoton laser scanning tomography[10], while approaches based on RCM have shown promise in automating computational assessments of photoaging through mathematical descriptor image analysis[11], opening avenues for data-driven quantification of skin aging with RCM[12].

The emergence of Line Field Confocal Optical Coherence Tomography (LC-OCT) has established itself as a powerful medical 3D imaging tool for in vivo optical biopsies of human skin. It supports the diagnosis of various skin disorders such as carcinomas[13], melanocytic skin tumor[14], inflammatory diseases[15], and actinic keratosis[16]. LC-OCT offers an isotropic spatial resolution of approximately 1 µm[17], enabling both vertical (B-scan) and en face (horizontal or C-scan) section imaging, and provides comprehensive 3D examinations of healthy skin[18]. Notably, its depth of analysis extends up to 500 µm, allowing characterization of the matrix of the superficial dermis of human skin. Previous studies have highlighted the capabilities of LC-OCT coupled with Artificial Intelligence (AI) for investigating the intricacies of healthy skin and age-related modifications at histological and cellular levels[19]. Segmentation algorithms facilitate the derivation of a range of 3D quantitative metrics, encompassing measurements of skin layer thicknesses, including the stratum corneum (SC) and epidermis, as well as detailed information concerning the keratinocyte network, including nuclei size, shape, density, and atypia[20]. However, while LC-OCT can determine superficial dermal thickness[21], additional information about the collagen network remains to be fully elucidated. In a separate study, Breugnot et al. focused on examining structural features of collagen in the superficial dermis employing deep learning techniques to classify the quality of collagen into four arbitrary classes defined by experts. However, no prediction of age was attempted in the study[22]. Ayadh et al. investigated the correlation between skin relief and fibrous network characteristics through qualitative morphological characterization of collagen under mechanical folding applied to the skin surface[23]. Most commonly, and as illustrated in the study by Bonnier et al., descriptive statistical analysis is performed on the quantitative metrics to highlight correlations with age-related modifications[24].

Despite the growing number of studies reported in the literature that utilize RCM, MPM and LC-OCT techniques, there has been no investigation to date that determines individual age by coupling these non-invasive tomographic imaging techniques with machine learning algorithms to leverage the information within different skin layers, such as the superficial dermis and its fibrous network. Therefore, this work represents the first demonstration of estimating age using a 3D ResNet-18 network as an AI-based analysis protocol to construct a model from LC-OCT 3D images of the superficial dermis. The deep learning algorithm was applied to a dataset consisting of 100 healthy Caucasian female volunteers aged between 20 and 70 years, who were enrolled in an exploratory clinical study of facial aging[24].

Results

Assessment of facial aging through clinical scoring

Table 1 displays parameters obtained from clinical scoring of each healthy Caucasian female participant enrolled in the current study. Firmness, plumpness, and elasticity were scored on a scale from 0 (not observed) to 10 (highest), while density ranged from 0 (not dense) to 11 (dense), and wrinkles appearance from 0 (none) to 6 (significant wrinkles). The analysis revealed a significant correlation between wrinkles and aging (P value < 0.001), showing an increase from 0.2+/-0.2 for the [20,30] age group to 4.2+/-1.3 for the [60,70] age group. Multiple comparison tests indicated statistically significant differences between most age groups, except for the age groups [40,50] and [50,60], which were not differentiated. Conversely, firmness, density, plumpness, and elasticity all exhibited a significant decrease with age ($p < 0.001$). These four parameters displayed similar trends, with firmness ranging from 8.6+/-1.4 to 2.2+/-1.6, density from 8.9+/-1.1 to 3.4+/-1.5, plumpness from 9.4+/-0.8 to 2+/-1.4, and elasticity from 9.6+/-0.6 to 2.1+/-1.6. Similarly, the multiple comparison test consistently differentiated between the youngest and oldest age groups, while the age groups [40,50] and [50,60] were not significantly different, except for plumpness. Clinical scoring remains a relevant approach to observe the macroscopic signs of aging by scoring key parameters. The evolution of the five parameters currently evaluated confirmed the presence of perceived modifications correlated with skin aging. Although clinical scoring does not directly assess the underlying fibrous network, the connection of firmness and elasticity with collagen and elastin organization is well established[25,26].

Figure 1 shows the regression of the predicted age using clinical scores against the chronological age for each volunteer. Presently, Multiple Linear Regression (MLR) was applied using the five assessed parameters, yielding a Mean Absolute Error (MAE) of 4.9 years and a Root Mean Square Error (RMSE) of 5.7 years, with a

Parameters		[20,30]	(30,40]	(40,50]	(50,60]	(60,70]	Test
Wrinkles	Mean (sd)	0.2 (0.2)	0.5 (0.3)	1.8 (1.6)	2.5 (1.7)	4.2 (1.3)	$p<0.001$ (Kruskal Wallis)
	Med [Q1-Q3]	0 [0-0.4]	0.4 [0.4–0.6]	1 [0.6–2.7]	2.2 [1-3.7]	4.5 [3.5–5.1]	
	Min-Max	0-0.4	0–1	0.4–4.6	0.4-6	1.4-6	
	Mult. comp.	a	b	c	c	d	
Firmness	Mean (sd)	8.6 (1.4)	6.8 (1.6)	4.7 (2.5)	3.5 (2.4)	2.2 (1.6)	$p<0.001$ (Anova)
	Med [Q1-Q3]	9 [7–10]	7 [6–8]	4 [3–6]	3.5 [1.8-6]	2 [1.8-3]	
	Min-Max	6–10	4–10	0–10	0–7	0–7	
	Mult. comp.	a	b	c	cd	d	
Density	Mean (sd)	8.9 (1.1)	7 (1.2)	5.6 (2.3)	4.2 (2.6)	3.4 (1.5)	$p<0.001$ (Anova)
	Med [Q1-Q3]	9 [8–10]	7 [6.8-8]	5 [4-7.2]	4 [2.8–6.2]	3 [2–4]	
	Min-Max	7–10	4–9	2–10	0–8	1–6	
	Mult. comp.	a	b	bc	cd	d	
Plumpness	Mean (sd)	9.4 (0.8)	7.5 (1.3)	5.3 (1.9)	3.4 (1.9)	2 (1.4)	$p<0.001$ (Anova)
	Med [Q1-Q3]	10 [9–10]	7.5 [7–8]	5 [4–7]	3 [3–5]	2 [1–3]	
	Min-Max	7–10	4–10	1–9	0–6	0–4	
	Mult. comp.	a	b	c	d	e	
Elasticity	Mean (sd)	9.6 (0.6)	7.8 (1.2)	5 (2.5)	4.4 (2.8)	2.1 (1.6)	$p<0.001$ (Anova)
	Med [Q1-Q3]	10 [9–10]	8 [7–9]	4 [3-6.2]	5 [2.5-7]	2 [1–3]	
	Min-Max	8–10	5–10	1–10	0–8	0–6	
	Mult. comp.	a	b	c	c	d	

Table 1. Summary of clinical parameters scored for statistical analysis. The 'Test' column indicates the significance of the effects of aging according to age groups for each parameter, providing the statistical method applied and the corresponding p-values. Letters indicate the outcomes from multi-comparison tests (when relevant).

Pearson correlation coefficient of 0.92. Table 2 summarizes the absolute relative errors for the 100 volunteers. The minimum and maximum absolute errors were 0.2 years and 14.2 years, respectively. It was observed that, in terms of distribution, 53 out of the 100 volunteers had a predicted error of less than 5 years when comparing chronological age to predicted age. Additionally, 42 volunteers had an error within a range of 5 to 10 years, and only 5 volunteers had a difference ranging from 10 to 15 years. With a mean relative error equal to 4.9 years, the correlation between clinical scores and chronological age is decent considering the low number of variables. It provides an overall representation of trends in clinical signs of aging based on clinical assessments.

Predicting individual age using LC-OCT 3D features of the dermis fibrous network

For the purpose of the study, a predictive model using deep learning has been trained on the dataset composed of 900 3D stacks collected from the temple, cheekbone, and mandible of 100 healthy women. AI-predicted age was computed using a Region Of Interest (ROI) located within the superficial dermis to encompass all features of the 3D fibrous network. The detailed procedure provided in the Methods section describes the cross-validation implemented that through iterations generates subsets of images used as validation sets to predict the age of each individual. Figure 2 presents the deep learning predicted facial age for each female volunteer regressed against their respective chronological age. The model yielded a Mean Absolute Error (MAE) of 4.2 years, and a Root Mean Square Error (RMSE) of 5.1 years, with a Pearson correlation coefficient of 0.94. Table 3 summarizes the relative errors for the 100 volunteers. The minimum and maximum absolute errors were 0.0 years and 13.5 years, respectively. Of the volunteers, 69 out of 100 were predicted with an absolute error of less than 5 years compared to their chronological age. Additionally, 26 fell within a 5-to-10-year error range, and only 5 were within the 10-to-15-year error range. The mean relative error of 4.2 years highlights how 3D features from the fibrous network captured during training can construct a predictive model that correlates with variations in skin microstructures linked to aging.

Correlation between facial age prediction through clinical scoring and LC-OCT imaging of fibrous network

Figure 3 presents the age prediction from clinical scoring regressed against age prediction from LC-OCT coupled with deep learning. A robust correlation ($R=0.87$, $p<0.05$) underscored the relevance of both approaches in correlating changes in skin features, both macroscopic and microscopic, with facial aging. Clinical scoring included assessments of firmness, plumpness, density, elasticity, and wrinkle appearance, based on visual inspection and palpation, resulting in an RMSE of 5.7 years. Conversely, the AI approach applied to LC-OCT images provided structural information about the superficial dermal fibrous network, resulting in a reduced RMSE of 5.1 years. However, deviations from chronological age, that is, errors in age prediction, when considering each volunteer individually did not yield a high correlation ($R=0.2$, Pearson). Beyond the complexity of the aging process, dermatologists can take into account holistic aspects of aging, resulting in a contrast between the objectivity of instrumental measurements and the subjectivity of clinical scoring, which relies on clinician experience and

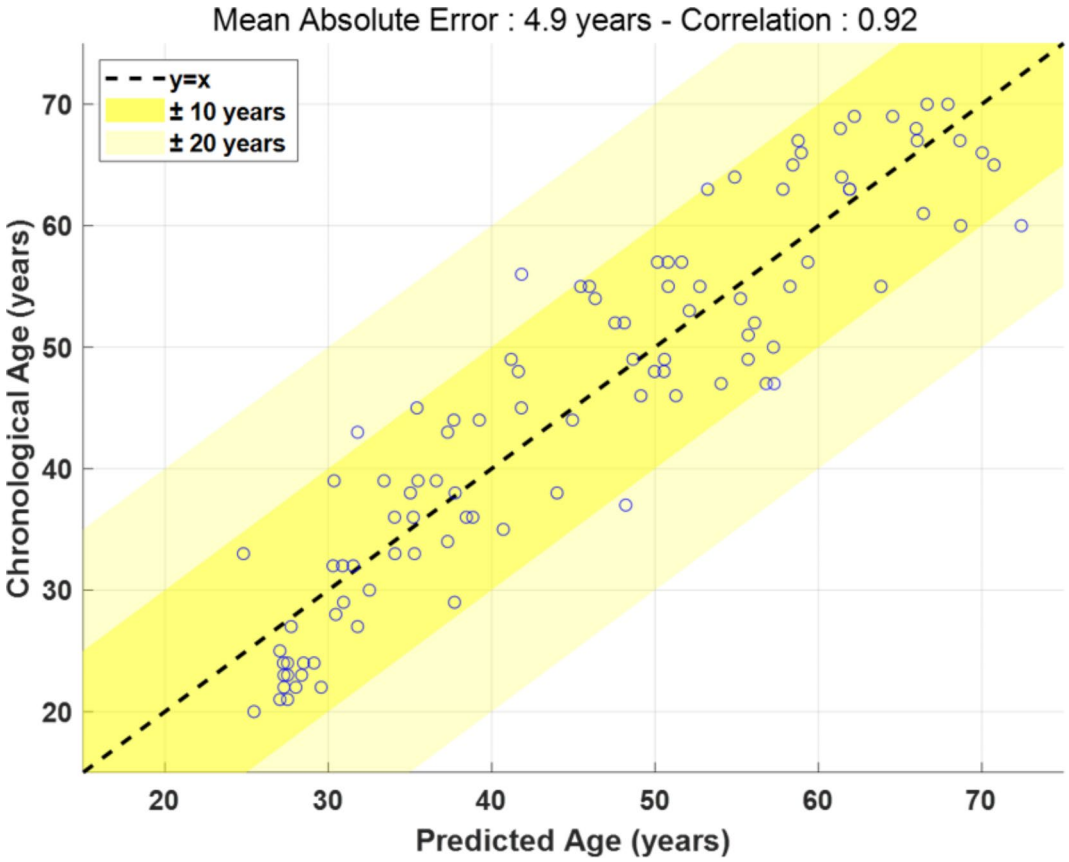

Fig. 1. Chronological age regressed against predicted age using Multiple Linear Regression applied to clinical scores. The blue line represents the linear regression where predicted age equals chronological age (x = y). The shaded areas indicate ranges of ± 10 years and ± 20 years relative to the blue line.

Absolute error range	< 1 year	(1-2.5] years	(2.5-5] years	(5–10] years	(10–15] years
Volunteers' distribution in %	8%	20%	25%	42%	5%

Table 2. Distribution of absolute errors, expressed in years, between chronological age and age predicted using multiple Linear regression (MLR) applied to clinical scores. Mean absolute error = 4.9 years. Min absolute error = 0.2 year. Max absolute error = 14.2 years.

perception. Additionally, factors such as instrument sensitivity, variation in facial areas assessed, and nuances in data interpretation further complicate the correlation of individually predicted age errors.

Discussion

Skin aging and associated clinical signs

Chronological aging and photoaging processes are known to lead to numerous cellular, molecular, and structural changes within the dermis and its fibrous network. The secretion of senescence-associated secretory phenotype (SASP) by senescent fibroblasts results in decreased cell proliferation due to impaired release of growth factors, and increased degradation of the extracellular matrix (ECM) through the activation of matrix metalloproteinases (MMPs). These changes ultimately contribute to irreversible skin aging, characterized by a decline in collagen density, thickness, and organization[27]. Moreover, collagen degradation, facilitated by increased MMPs and decreased levels of tissue inhibitors of metalloproteinases (TIMPs), exacerbates oxidative stress within damaged cells, further accelerating skin aging. Similarly, elastic fibres undergo structural changes during aging, with fibrillin-rich microfibrils in the papillary dermis selectively disintegrating. The expression of fibulin-5 (FBLN5), crucial for elastic fibre remodelling, diminishes with age, particularly in photo-protected skin[28]. Photoaged skin also manifests histological features such as heterogeneous epidermal rete ridge thickness and solar elastosis. The latter is characterized by thickened, curled, and fragmented elastic fibres, primarily attributed to MMP activation. Additionally, reduced synthesis of new elastic fibres contributes to the loss of skin elasticity in photoaged skin. Changes in the ECM are closely linked with functional alterations characteristic of both intrinsic aging and photoaging, such as a reduction in elasticity, an increase in wrinkles and sagging, and a

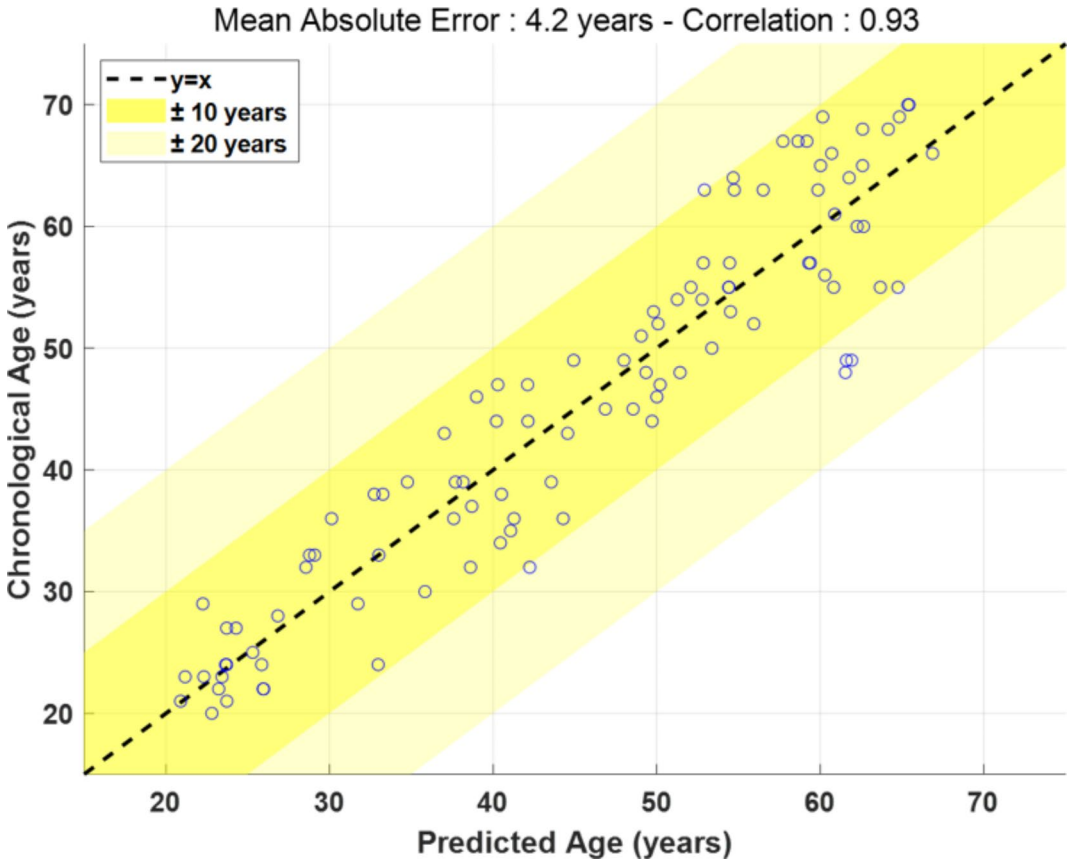

Fig. 2. Chronological age regressed against predicted age using deep learning algorithms on LC-OCT images. The blue line represents the regression line where predicted age equals chronological age (x = y). The shaded areas indicate ranges of ± 10 years and ± 20 years relative to the blue line.

Absolute error range	< 1 year	(1-2.5] years	(2.5-5] years	(5–10] years	(10–15] years
Volunteers' distribution in %	12%	21%	36%	26%	5%

Table 3. Distribution of absolute errors, expressed in years, between chronological age and age predicted using deep learning analysis applied to LC-OCT 3D images. Mean absolute error = 4.2 years. Min absolute error = 0.0 year. Max absolute error = 13.5 years.

decrease in skin firmness. Clinical scoring by dermatologists enables the measurement of these macroscopic signs of facial aging in vivo, as performed in the present exploratory study involving a cohort of 100 healthy Caucasian women. The clinical evaluations confirmed a significant reduction across different age groups in skin elasticity (from 9.6 ± 0.6 to 2.1 ± 1.6), firmness (from 8.6 ± 1.4 to 2.2 ± 1.6), and density (from 8.9 ± 1.1 to 3.4 ± 1.5) as noted in Table 1. Visually assessed indicators such as wrinkles also reveal macroscopic changes due to aging, with wrinkle scores increasing from 0.2 ± 0.2 to 4.2 ± 1.3 across the age spectrum from [20-30] to [61–70] years old. Similarly, a decline in plumpness with age, from scores of 9.4 ± 0.8 down to 2 ± 1.4, is another perceptible sign of aging that reflects alterations within the skin's microstructures. Expert assessment allows these visible signs of facial aging to be quantitatively scored on a global scale, providing valuable insights into the extent of age-related variations within the skin's appearance and structure. Moreover, this study's observations, which included volunteers ranging from 20 to 70 years old, confirm that significant effects of aging are encompassed within the studied panel, thereby validating its use for more detailed investigations into skin microstructures using advanced methods like 3D imaging.

Deciphering signs of aging in vivo using non-invasive imaging techniques

While assessing molecular information non-invasively remains challenging compared to in vitro or ex vivo experiments with explants, imaging techniques such as LC-OCT enable the capture of histological and morphological changes resulting from cellular and protein-level alterations (fibrous network). In vivo skin imaging encompasses various techniques aimed at characterizing subsurface structures with varying degrees of resolution[29]. HFUS (High-Frequency UltraSounds), OCT, RCM, MPM, and more recently, LC-OCT, are a subset

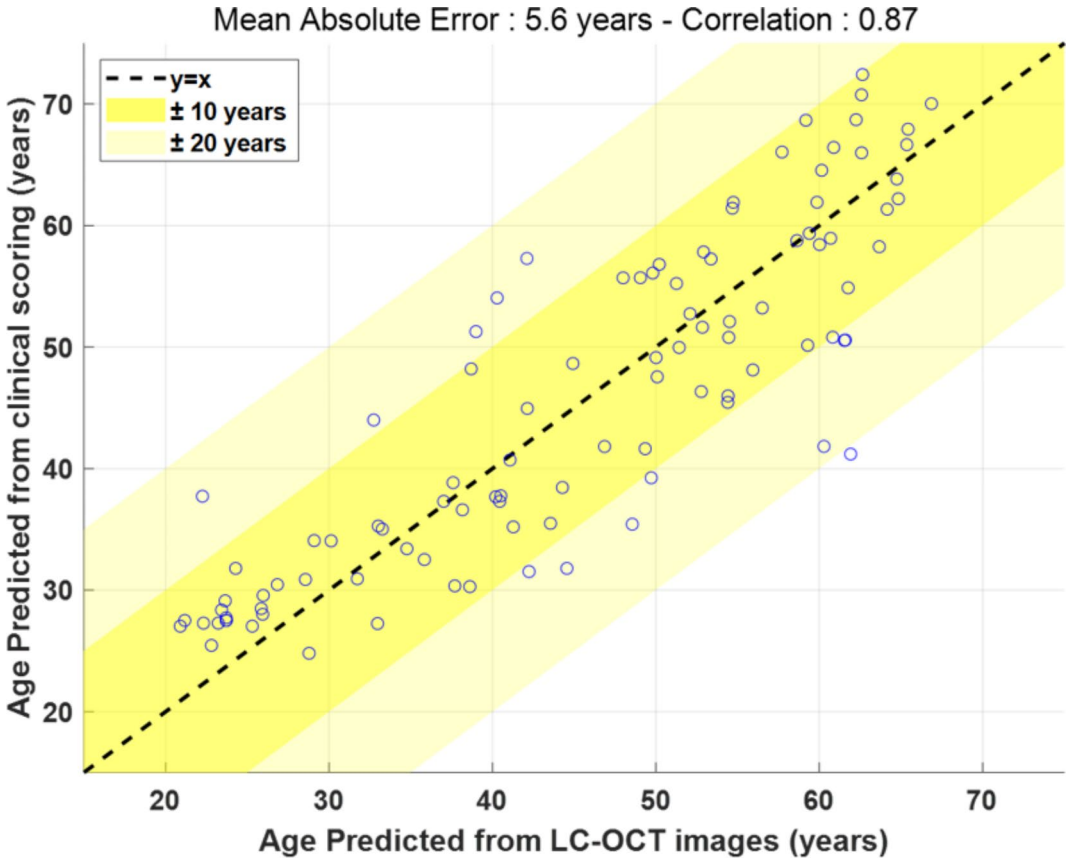

Fig. 3. Age predicted from clinical scoring regressed against age predicted from LC-OCT images. The blue line represents the regression line where predicted age equals chronological age (x = y). The shaded areas indicate ranges of ± 10 years and ± 20 years relative to the blue line.

of the technologies commonly employed and compared within this domain. These techniques were initially designed for diagnosing pathologies[30], but there is growing interest in exploratory studies involving healthy skin[7,31]. The overarching goal remains consistent: to quantify modifications occurring within the skin layers. HFUS and OCT have been pivotal in non-invasive imaging, enabling the visualization of skin cross-sections for measuring thickness and morphological alterations[32]. Notably, the subepidermal low-echogenic band (SELEB) has emerged as a marker of aging, underscoring the significance of these imaging modalities in understanding age-related skin changes[33]. Nowadays, HFUS remains a rapid and cost-efficient tool for evaluating the efficacy of anti-aging treatments in vivo[34].

RCM has pioneered the concept of microscopic optical biopsies and garnered significant attention for its observation of skin features. It provides access to quantitative biomarkers through histological observation[6], such as epidermal thickness (including stratum corneum, suprapapillary epidermis, rete ridges, and entire epidermis), furrow aspect (ranging from not visible to disarranged), furrow width (narrow or wide), furrow distance, extension of irregular honeycomb pattern of the epidermis, mottled pigmentation of the epidermis, polycyclic papillary contours of dermal papillae, presence of dermal papillae, and type of dermal collagen (curled, huddled, coarse, and thin reticulated)[35]. Several studies in the literature provide descriptive data on photoaging, further emphasizing the utility of grading skin aging processes using RCM[36]. As far back as 2006, in vivo characterization of skin aging has been studied using MPM for the visualization of ECM such as collagen and elastin through autofluorescence and second harmonic generation measurements[37]. More recently, 3D imaging for multiparametric quantification of aging[9] and even cell-specific studies of mast cells in the dermis[38] have also been reported.

LC-OCT has increasingly gained attention for skin imaging in dermatology and the study of aging in healthy volunteers[39]. Monnier et al. reported its potential by comparing different body sites (cheek, tip of the nose, upper chest, posterior forearm, and back) to determine the thickness of the stratum corneum (SC) and viable epidermis from 10 healthy volunteers[39]. In 2021, Chauvel-Picard et al. further emphasized the characterization of healthy epidermis by coupling 3D LC-OCT with a similar approach, comparing 7 body sites[20]. Despite the limited sample size, the work by Chauvel-Picard et al. highlighted the variability observed on the face, notably between the forehead (SC = 11.6+/-2.5 µm and epidermis = 69.4+/-11.8.7 µm) and the nose (SC = 13.0+/-3.4 µm and epidermis = 76.4+/-9.6 µm), which were found to have significantly thicker superficial layers compared to the cheek (SC = 9.7+/-1.6 µm and epidermis = 49.7+/-4.2 µm). This study initiated reflection on the relevance of the technique to study age-related modifications through quantitative cellular and histological

metrics calculated from LC-OCT images. Bonnier et al. conducted an exploratory study, further emphasizing the identification of facial aging biomarkers in female Caucasian volunteers through LC-OCT. Specifically, they observed modifications in the number of cell layers, decreased cell surface density, nuclei volume, and enhanced cell network atypia[24]. LC-OCT facilitates 3D imaging at depths of up to 500 µm, allowing for the visualization of the fibrous network within the superficial dermis. Breugnot et al. examined dermal quality in a clinical study involving 57 healthy Caucasian female volunteers between 22 and 79 years old, aiming to classify images into four classes based on dermatological observations grading the fragmentation of fibrous structures as opposed to the reticulated conformation[22]. A correlation between the classification of LC-OCT images and age, as well as between photo-exposed and non-photo-exposed groups was demonstrated, highlighting the potential to characterize collagen within the superficial dermis. In a separate study, Ayadh et al. investigated the relationship between skin relief and dermal fibrous structures using folding tests in 42 French Caucasian women volunteers divided into a young group[20–30] years old and a middle-aged group (45–55 years old), illustrating how information about the superficial dermis could unveil fibrous orientation and density[23]. Nevertheless, exploration of the dermal fibrous network (collagen network) within the context of aging remains scarce, notably due to the recent emergence of the technique.

AI-based image analysis to investigate effects of aging in vivo

Non-invasive imaging techniques provide a particularly relevant means to access information about aging-related changes from the surface to the deeper layers of skin. RCM[12], MPM[9], and LC-OCT[24], when paired with AI and computer vision techniques, have been repeatedly reported to describe, quantify, and correlate the effects of aging with biological metrics. These studies commonly aim to provide automated images analysis that is comparable to observations made by dermatologists. For instance, Hames et al.[40] used K-means clustering and zero component analysis (ZCA) to identify four distinct anatomical layers of the skin: the stratum corneum, viable epidermis, dermal-epidermal junction, and papillary dermis. Pena et al.[9] applied automated segmentation methods to z-stacks from combined two-photon excitation fluorescence-lifetime imaging microscopy (2PEF-FLIM), utilizing morphological watershed and graph cuts algorithms while accounting for the actual shape of the skin surface and the dermal-epidermal junction. Bonnier et al.[24] reported quantitative metrics derived from LC-OCT images using a 2D U-Net model for histological analysis and a 3D StarDist model for cellular metrics[41]. AI is a relevant tool for facilitating the segmentation of skin layers and microstructures, such as cells. Although various methods have been proposed in the scientific literature[42], there is currently no consensus on optimal approach or a standard protocol. Comparing these methods' results against dermatologists' assessments[43] or ex vivo approaches that combine non-invasive measurements with histological examination of stained Sect[21] can reinforce confidence in these computational techniques. However, due consideration should be given to differences in optical properties which may limit correlation at times[44]. Recently, much research has focused on automating segmentation processes with novel approaches investigating real-time segmentation of OCT images using computationally efficient convolutional neural network-graph search algorithms (CNN-GS)[45]. Indeed, integrating AI with image analysis and machine learning offers extensive applications in healthcare, opening up a broad spectrum for research[46]. AI-driven tomographic image analysis systems enhance medical diagnostics, pathology investigation, and radiology interpretations by enabling faster and more precise diagnoses[47].

Machine learning for predicting individual age

The burgeoning field of AI and machine learning has strengthened the assessment of biological age, with the analysis of diverse biomarkers becoming a focal point across various scientific disciplines[48]. These biomarkers range from blood sample analyses[49] to the application of genomics in skin cell research[50]. As technology and methodology advance, researchers are exploring varied approaches to accurately predict an individual's age, notably through non-invasive sampling methods. Nevertheless, despite the proliferation of AI and computer vision techniques coupled with imaging methods, to the best of our knowledge, no other study in the literature aims to predict an individual's chronological age using in vivo microscopic skin imaging combined with deep learning models. Therefore, comparisons of the currently reported approach to others in the field can only be made against different documented methods such as full-face imaging (photography), where specific facial features are analysed through machine learning algorithms. For instance, Bobrov et al. developed a predictor of chronological age called the PhotoAgeClock, which relies on visual photographic biomarkers of aging applied from anonymized images of eye corners from a population aged between 20 and 80 years old. Deep neural networks trained on 8414 high-resolution images, each labelled with the correct chronological age, yielded a mean absolute error of 2.3 years[51]. Park et al. revealed the findings of their study, which involved a deep learning-based system utilizing SSR-Net (Soft Stagewise Regression Network). This system was trained on 11,000 facial images collected from Korean volunteers aged 19 to 79, aimed at diagnosing facial aging. Their model enabled the prediction of chronological age with an error margin of approximately ± 3 years[52]. ElKarazle et al. provided an overview of facial age estimation using machine learning techniques. The authors notably discussed the strengths and limitations of age estimation models, which were categorized as handcrafted and deep learning-based models. Deep learning facial extraction methods using algorithms such as convolutional neural networks (CNNs) or multilayer perceptrons (MLPs) were discussed. Examples of commonly used pre-trained networks and studies reported a MAE between 2 and 8 years. The MAE varied depending on the initial dataset used to train the model, the algorithm used, and the parameters set to apply the algorithm[53]. While predicting age from pictures of full faces has been investigated for quite some time, the performance of predictive models has improved through large datasets comprising thousands of photographs. Interestingly, predictions currently achieved with LC-OCT fall within the 2 to 8 years MAE range reported by Elkhaze et al. Present results are encouraging, suggesting that the performance of predictions through LC-OCT could be further increased when broader datasets, such as those from shared banks of photographs, become available. In a study by Cho et al., applying the cforest model

to predict the age of Korean women using various biophysical properties combining biomechanical properties, skin appearance and biometric measurements yielded an $R^2 = 0.799$ and RMSE = 6.222[54]. Other sophisticated methods have been developed to explore the relationship between DNA methylation (DNAm) levels at CpG sites and chronological age using samples from blood, teeth, and bone. Dias et al. reported results from the Multi-Tissue BBT-APM model, utilizing Sanger sequencing, that yielded at best a Mean Absolute Deviation (MAD) of 6.09 years (Root Mean Square Error (RMSE) = 7.55) on the training set. When applied to the validation set, the model achieved a MAD of 6.08 years (RMSE = 7.64)[55]. Estimating and predicting age remains an active field of research. To date, no method, regardless of its complexity, has consistently produced error margins narrower than a few years. Thus, integrating microscopic imaging with deep learning models emerges as a promising strategy for calculating an individual's age based on skin biomarkers within the dermis. The successes reported in current studies offer new outlooks on understanding the process of skin aging and provide effective ways to quantify and monitor it.

Conclusion

In vivo 3D Line-field Confocal Optical Coherence Tomography (LC-OCT) imaging has emerged as a powerful tool for extracting critical information about underlying skin microstructures. For instance, when integrated with deep learning algorithms, it is a potent predictive tool for determining age by analysing variations in the dermal fibrous network. Optimization of the 3D ResNet model and thorough cross-validation using a dataset collected from a cohort of 100 healthy Caucasian female volunteers achieved a Mean Absolute Error (MAE) of 4.2 years with a Pearson correlation coefficient of 0.93. This significant accuracy achieved in vivo for predicting chronological age offers profound insights into the capability to capture features non-invasively, reflecting structural changes that occur within the skin as it ages. Moreover, its correlation with clinical signs of aging such as elasticity, firmness, or wrinkles assessed through clinical scoring ($r = 0.87$) opens up new pathways for comprehensive studies into the aging process at both macroscopic and microscopic levels. AI-assisted analysis, i.e., deep learning, is a critical tool for pushing the boundaries of in vivo imaging like LC-OCT; therefore, it represents a valuable asset to decipher the effects of aging in deeper layers of the skin and their visible outcomes that shape our perception of aging.

Methods

Study population

The study was conducted in accordance with local (France) legal regulations and in adherence to the principles outlined in the Declaration of Helsinki. Research approval was obtained from the French Ethical Committee "Comité de protection des personnes sud méditerranée I" (IDRCB: 2021-A00101-40). Prior to participation, all volunteers provided written informed consent. The cohort consisted of one hundred healthy Caucasian female volunteers, classified according to the Fitzpatrick scale into skin phototypes I, II, or III (Table 4). Participants were evenly distributed across five age groups: [20–30], [31–40], [41–50], [51–60], and [61–70]. Each volunteer's chronological age, documented on their personal identification, was utilized as input for the construction of predictive models. Additionally, a trained assessor conducted clinical scoring on facial features to assess skin firmness, density, plumpness, elasticity, and the presence of crow's feet wrinkles. The side of the face evaluated (left or right) was determined randomly. The clinical scoring process involved standardized positioning and lighting conditions to ensure consistency and accuracy.

LC-OCT 3D imaging

3D LC-OCT images were acquired using the DeepLive™ system (DAMAE MEDICAL, France). This system captures images measuring 1200 µm x 500 µm in the x and y directions and up to 500 µm in depth (z), with an isotropic cellular resolution of approximately 1.3 µm. This resolution enables detailed visualization of microstructures within the superficial dermis, specifically the fibrous network. The DeepLive™ system also features a secondary optical path for real-time visualization of a colour surface image of the skin, aiding in the guidance of LC-OCT acquisition.

Detailed characteristics of DeepLive™ and LC-OCT can be found in the literature[56–58]. Each 3D image is automatically reconstructed from a series of horizontal 2D images during acquisition. The depth scanning speed is set such that the 2D images in the series are all separated by $\Delta z = 1$ µm, consistent with the resolution of LC-OCT, resulting in 3D images reconstructed from 350 horizontal 2D images. As the acquisition speed of the horizontal 2D images is 8 frames per seconds, the duration of acquisition of the 3D images is approximatively 45 s. Presently, for each volunteer, three LC-OCT images were acquired from the temple, cheekbone, and mandible (lower jawline), with a separation of approximately 1–2 mm between acquisitions. Pigmented areas were deliberately avoided. A randomization method determined which side of the face (left or right) was analysed

Phototype	[20–30]	[31–40]	[41–50]	[51–60]	[61–70]
I	2	0	1	3	1
II	8	8	7	7	3
III	10	12	12	10	16
Total	20	20	20	20	20

Table 4. Distribution of phototypes by Fitzpatrick skin type across studied age groups.

for each participant. The resulting dataset comprised 900 3D image stacks, evenly distributed across age groups, facial areas and participants (180 images per age group, 60 images per facial area, nine images per participant).

Statistical analysis

The clinical scores were reported as mean +/- standard deviation. An ANOVA was carried out in order to compare subjects across age groups. The normality of the ANOVA residuals was assessed by the Shapiro-Wilk test, with a significance level set at 10%. If normality of the residuals was not verified, a Kruskal-Wallis (KW) test was used as an alternative. When either ANOVA or KW test was significant, multi-comparison tests were performed to compare age groups pairwise, with Tukey adjustment for multiple comparisons. Linear correlations were measured using the Pearson correlation coefficient. Letters assigned to each age group illustrate their discrimination and visualize significant variations in metrics with age. The level of significance for all statistical analyses was set at $p < 0.05$.

Age prediction model using clinical scoring: multiple Linear regression analysis

Age prediction was performed using Multiple Linear Regression (MLR) based on the clinical scores. MLR is a statistical method that models the relationship between a dependent variable (in this case, chronological age) and multiple independent variables (clinical scores). The generalized regression model is expressed as:

$$\text{Age} = \beta_0 + \beta_1 \times \text{Score}_1 + \beta_2 \times \text{Score}_2 + \beta_3 \times \text{Score}_3 + \ldots + \beta_n \times \text{Score}_n + \varepsilon$$

where β_0 is the intercept, β_1, β_2, β_3, …, β_n are the regression coefficients for each clinical score, and ε is the residual error. The model parameters (β_0, β_1, β_2, β_3, …, β_n) were estimated using the least squares method, which minimizes the sum of the squared residuals. The accuracy of the predictions was evaluated using the Mean Absolute Error (MAE) and the Root Mean Square Error (RMSE). The Pearson correlation coefficient was calculated to assess the linear relationship between the predicted ages and the chronological ages.

Dermis-epidermis junction (DEJ) detection

There is interindividual variability in skin structures characterized by varying thicknesses in the stratum corneum and viable epidermis. Therefore, the initial step of data preparation consists of detecting the position of the Dermal-Epidermal Junction (DEJ) to focus image processing on the superficial dermis hence the collagen network. Segmentation of images was performed using Python (Welcome to Python.org). 3D Slicer (version 4.11 https://www.slicer.org/) and ImageJ (version 1.54f https://wsr.imagej.net/notes.html) were employed for preparing Figs. 4, 5, and 6, respectively. Presently, the skin layers segmentation model used is a 2D UNet architecture, applied on the two vertical axes (x and y) of each 3D stack, corresponding to 500 + 1200 2D image inferences. The average of all the predictions generates a 3D segmentation of the DEJ as illustrated in Fig. 4. Areas corresponding to hair follicles were excluded from the calculation of the mean DEJ position. Further details about the skin layers segmentation algorithm can be found in published studies[24,59].

Dermis region of interest (ROIs)

To develop predictive age models using deep learning algorithms based on features associated with the collagen network, it is essential to initially generate data inputs corresponding to the superficial dermis, subsequently referred to as the region of interest (ROI). The ROIs used as inputs for the deep learning algorithm need to be right rectangular prisms. Presently, they are 3D sub-stacks extracted from the LC-OCT 3D stacks (images). As

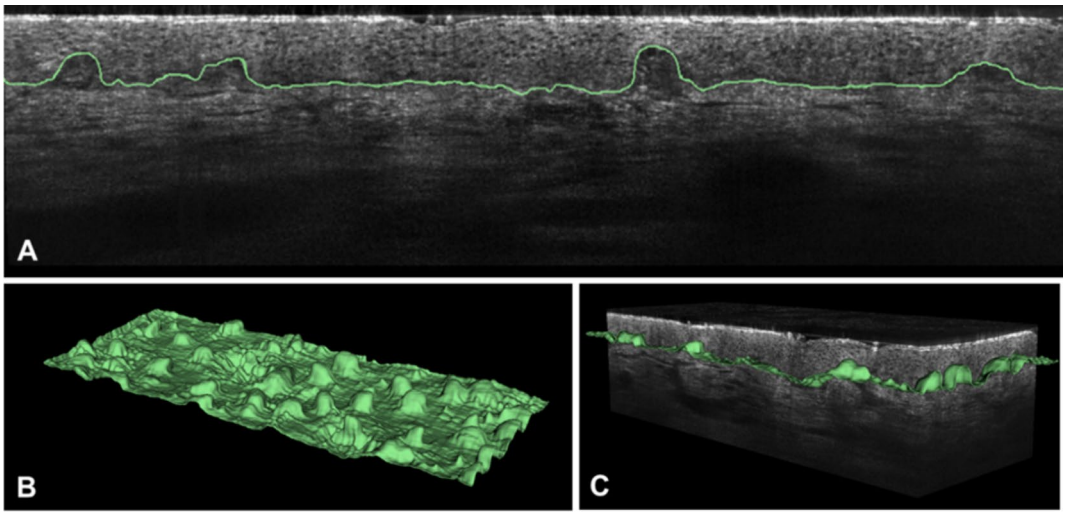

Fig. 4. Segmentation of the DEJ. (A) Reconstructed 2D vertical image showing the DEJ segmentation. (B) Illustration of the DEJ segmentation mask in 3D. (C) Overlay of the DEJ segmentation mask on the 3D LC-OCT stacks for subsequent selection of the Region of Interest (ROI).

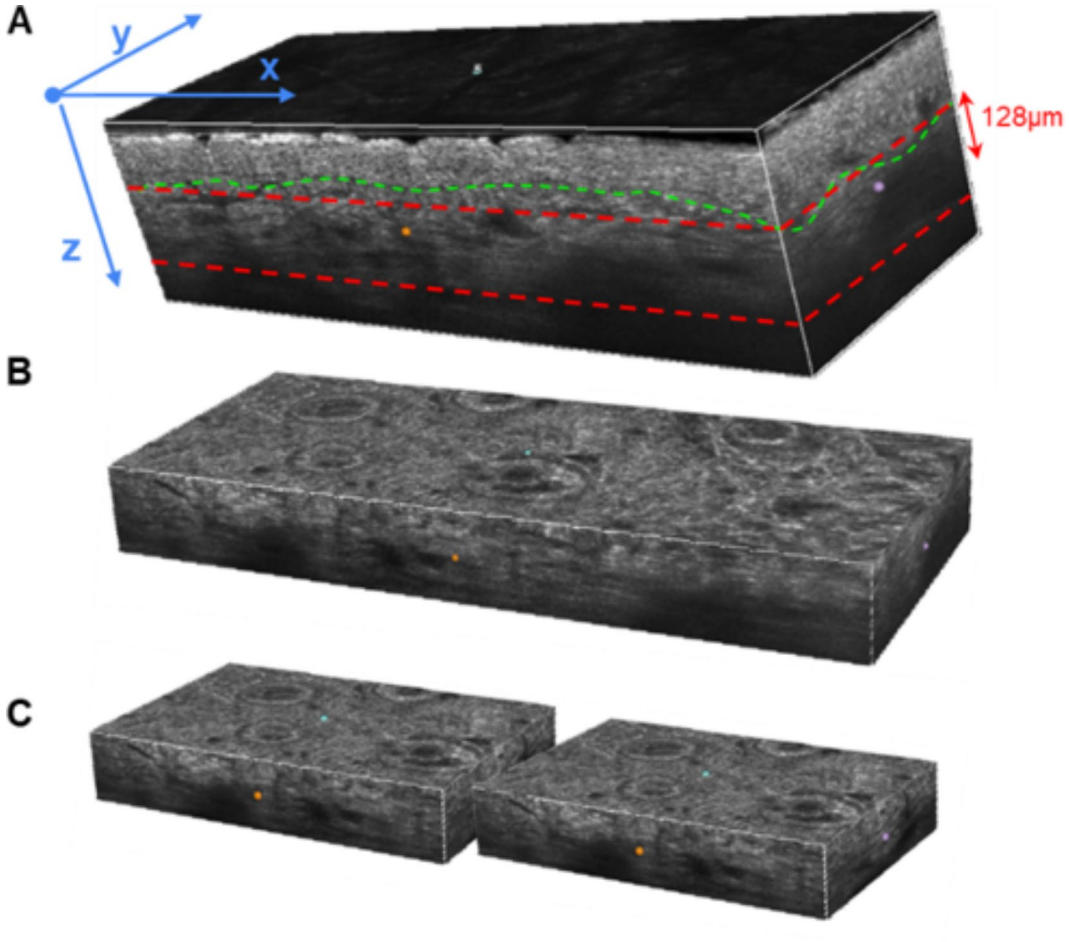

Fig. 5. Preprocessing steps: a- Original LC-OCT 3D acquisition with DEJ segmentation (green) and start - end of the region of interest (red) b- Extracted region of interest c- Down sampled tiles for predictions.

illustrated in Fig. 5, for a given 3D stack k, the average depth of the DEJ (zk_{dej}) was computed using the above-mentioned skin layers segmentation algorithm. The ROI is then defined as the entire sub-stack starting at depth $Zk_{start} = Zk_{dej} + 5$ µm and ending at depth $Zk_{end} = Zk_{start} + 128$ µm. A step-by-step approach utilizing the thickness of the sub-stack was employed to refine the region of interest (ROI) to 128 µm within the z-dimension, which appeared optimal for the current deep learning model used to predict the age of the fibrous network within the superficial dermis (data not shown).

Preparation of training inputs for 3D convolutional neural networks

The dermis fibrous ROIs are by designed of size $1200 \times 500 \times 128$ µm^3 at native resolution. It should be noted that images are recorded with a pixel size of 1 µm in all directions, meaning that the number of pixels corresponds to the dimensions. Since 3D models are particularly resource-intensive in terms of graphics processing unit (GPU) RAM, the size of the input images for training a 3D deep learning model is often constrained by the available computing resources. Training models at full resolution was not feasible due to GPU memory constraints; therefore, downsizing the 3D images by a factor of 2 and splitting them into two tiles was considered a good trade-off, balancing between training resolution and inference time. Currently, the 2-fold downsizing effectively reduces the resolution in images from $1 \times 1 \times 1$ µm^3 to $2 \times 2 \times 2$ µm^3, while significantly reducing the image size. Considering that the deep learning model is predominantly trained on features such as fibre organisation, density, and orientation, elements which remain intact within the processed images (as shown in Fig. 6), the downscaled images exhibit minimal degradation of information. They still enable clear visualization of the fibrous network given its mean horizontal diameter of 4–7 µm, which is significantly larger than the LC-OCT resolution of approximately 1.3 µm (Fig. 6). To further reduce the input sizes of the model without further degrading the resolution, each downscaled 3D image was split into 2 equal tiles overlapping on the longest axis x by 14 pixels after resizing, which corresponds to an overlap of 28 µm at full resolution (Fig. 5c). After preprocessing, the training data consisted of 1800 3D stacks of size $314 \times 250 \times 64$ pixels. A simple data augmentation scheme was used during training to add more training examples and improve the model's generalization capacity: tiles were randomly flipped along the x and/or y axis, effectively creating realistic samples that would not alter the depth axis z. To fully preserve the unique texture of the fibrous network, no other data augmentations were applied.

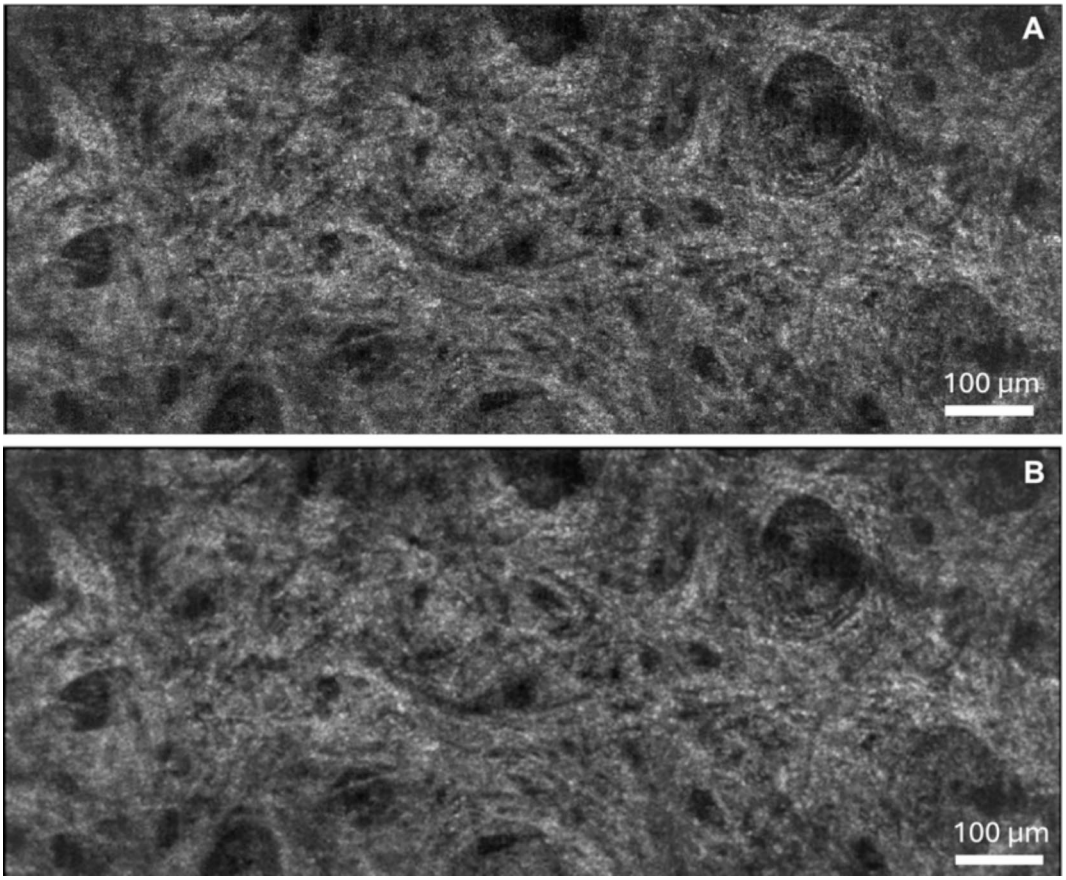

Fig. 6. Preprocessing steps. (A) An exemplary horizontal cross-section image extracted from a native resolution 3D LC-OCT stack. (B) The corresponding horizontal image after the application of a two-fold downscaling process.

Enhancing statistical robustness: five-fold cross-validation approach

To ensure statistical robustness, a five-fold cross validation (CV) split was performed by volunteers, following standard good practices. The dataset was randomly divided into five equal-sized subsets (i.e. folds). In this approach, all the acquisitions (3D LC-OCT images) for a given volunteer were either entirely in the training set or the validation set, but never in both. This ensures that a different validation set was used each time, preventing the model from overfitting on a fixed validation set. As a result, no early stopping was performed during each training session to select the best model, thus avoiding any overestimation of the model's performance. The model was then trained on four of the folds and tested on the fifth fold. This process was repeated five times, with each fold serving as the test set once while the other four folds were used for training. Performance metrics (such as accuracy, precision, etc.) were calculated for out-of-fold predictions in each iteration to obtain an overall assessment of the model's performance.

Training and implementation of the predictive model

In the initial phase of method development, a 2D convolutional model was employed. It was trained on horizontal cross-sections of the facial superficial dermis within the region of interest (ROI). For the final age prediction, the model outputted estimations for successively spaced images (at intervals of 5 µm), which were then averaged to produce a composite score. As reported in Table 5, significant improvement was achieved by optimizing training parameters and employing strategic data augmentation. This enhancement in the model's performance is reflected by improved cross-validation correlation scores at the stack level, rising from 0.590 to 0.633.

A significant increase in prediction accuracy was achieved by transitioning from conventional regression modelling to an optimization of age prediction via ordinal classification. Through an empirical approach, it was observed that the most successful models were developed by transitioning from conventional regression modelling to an optimization of age prediction via ordinal classification. The present study didn't aim to emphasize a theoretical advantage of one method over the other, however, it has been found that neural networks tend to train more effectively with cross-entropy loss as compared to mean squared error loss, and thus ordinal classification was preferred here. The investigation concentrated on a regression task that aimed to predict continuous numerical age values. Adopting an ordinal classification framework, rather than a traditional regression approach, improved predictive performance of 0.05 in stack-level correlation scores (Table 5). This ordinal approach discretizes age into four binary categories, Ca, delineated by age brackets: >30, > 40, >50, and

Experiment	Correlation
2D ResNet18 baseline	0.590
Parameters tweaking & data augmentation	0.633
Ordered classification	0.685
3 channels inputs	0.739
3D final approach	0.811

Table 5. Step wise training and implementation of the predictive model with corresponding improvements of correlation scores.

> 60 years. At the inference stage, the predicted probabilities for these categories, denoted as (pi)i ∈ Ca, were utilized to estimate age. The predictive age formula used was:

$$Page = 20 + 50 * \left(\frac{1}{4}\sum_{i=1}^{4} Pi\right)$$

This formula leverages the cumulative probabilities across the ordered categories, effectively transforming categorical outputs back into a continuous age prediction between 20 years and 70 years. Since 3D images were split into two by the preprocessing pipeline, the final age prediction for 3D images was the average of the scores of the two tiles.

Further significant enhancement was achieved (correlation = 0.739) by reformatting the grayscale image inputs, evolving from a single channel to a 3-channel input format, with each channel representing sequential image frames. This modification represented a preliminary step towards incorporating spatial depth, effectively laying the groundwork for a 3D analytical perspective.

The comprehensive 3D methodology demonstrated superior performance compared to the previous 2D techniques, solidifying the benefits of employing full three-dimensional convolutional modelling. This approach more effectively captures the complex spatial relationships within the dermal fibrous network, further improving the correlation to 0.811, as shown in Table 5. The model's architecture was inspired by the ResNet18 network but adapted to a 3D context, utilizing 3D convolutions instead of 2D ones as implemented in PyTorch by Hara et al. The model outputs four distinct probabilities through a sigmoid activation function. Models were trained in PyTorch (https://pytorch.org/) over 20 epochs using binary cross-entropy loss and the Adam optimizer with a linear learning rate decay to a maximum value of $1e^{-4}$ after a warmup period consisting of 5% of total iterations. The batch size was set to a maximum value of 16, allowing for training on an NVIDIA RTX 2080 Ti GPU.

Data availability

The data that support the findings of this study are not openly available due to reasons of sensitivity and are available from the corresponding author upon reasonable request.

Received: 3 July 2024; Accepted: 25 September 2024
Published online: 15 October 2024

References

1. Bielfeldt, S., Springmann, G., Seise, M., Wilhelm, K. P. & Callaghan, T. An updated review of clinical methods in the assessment of ageing skin – new perspectives and evaluation for claims support. *Int. J. Cosmet. Sci.* **40**, 348–355 (2018).
2. Dobos, G., Lichterfeld, A., Blume-Peytavi, U. & Kottner, J. Evaluation of skin ageing: A systematic review of clinical scales. *Br. J. Dermatol.Bold"*>*172*, 1249–1261 (2015).
3. Bazin, R. & Doublet, E. *Skin Aging Atlas*. (Med'com).
4. Vierkötter, A. et al. The SCINEXA: Anovel, validated score to simultaneously assess and differentiate between intrinsic and extrinsic skin ageing. *J. Dermatol. Sci.* **53**, 207–211 (2009).
5. Costello, L. et al. Quantitative morphometric analysis of intrinsic and extrinsic skin ageing in individuals with Fitzpatrick skin types II–III. *Exp. Dermatol.* **32**, 620–631 (2023).
6. Guida, S., Pellacani, G., Ciardo, S. & Longo, C. Reflectance confocal microscopy of aging skin and skin cancer. *Dermatol. Pract. Concept.* **11**, e2021068 (2021).
7. Chen, K., Wang, Z., Han, Y. & Cui, Y. In vivo detection of healthy skin: Comparison of multiphoton microscopy and reflectance confocal microscopy. *Ski Res. Technol.* **29**, e13340 (2023).
8. Pezzini, C. et al. Skin ageing: Clinical aspects and in vivo microscopic patterns observed with reflectance confocal microscopy and optical coherence tomography. *Exp. Dermatol.* **32**, 348–358 (2023).
9. Pena, A. M. et al. In vivo multiphoton multiparametric 3D quantification of human skin aging on forearm and face. *Sci. Rep.* **12**, 14863 (2022).
10. Koehler, M. J. et al. Morphological skin ageing criteria by multiphoton laser scanning tomography: Non-invasive in vivo scoring of the dermal fibre network. *Exp. Dermatol.* **17**, 519–523 (2008).
11. Raphael, A. P. et al. Computational characterization of reflectance confocal microscopy features reveals potential for automated photoageing assessment. *Exp. Dermatol.* **22**, 458–463 (2013).
12. Hames, S. C., Bradley, A. P., Ardigo, M., Soyer, H. P. & Prow, T. W. Towards data-driven quantification of skin ageing using reflectance confocal microscopy. *Int. J. Cosmet. Sci.* **43**, 466–473 (2021).
13. Donelli, C. et al. Line-field Confocal Optical Coherence Tomography for the diagnosis of skin carcinomas: Real-Life Data over three years. *Curr. Oncol.* **30**, 8853–8864 (2023).
14. Perez-Anker, J. et al. Criteria for melanocytic lesions in LC-OCT. *J. Eur. Acad. Dermatol. Venereol.*https://doi.org/10.1111/jdv.20079 (2024).

15. Orsini, C. et al. Line-field confocal optical coherence tomography: New insights for psoriasis treatment monitoring. *J. Eur. Acad. Dermatol. Venereol.* **38**, 325–331 (2024).
16. Ruini, C. et al. In-Vivo LC-OCT evaluation of the Downward Proliferation Pattern of keratinocytes in Actinic Keratosis in comparison with histology: First impressions from a pilot study. *Cancers* **13**, 2856 (2021).
17. Dubois, A. et al. Line-field confocal time-domain optical coherence tomography with dynamic focusing. *Opt. Express* **26**, 33534–33542 (2018).
18. Ogien, J., Levecq, O., Azimani, H. & Dubois, A. Dual-mode line-field confocal optical coherence tomography for ultrahigh-resolution vertical and horizontal section imaging of human skin in vivo. *Biomed. Opt. Express* **11**, 1327 (2020).
19. Río-Sancho, S., del, Gallay, C., Ventéjou, S. & Christen-Zaech, S. In vivo evaluation of skin of children with LC-OCT: An objective assessment. *J. Eur. Acad. Dermatol. Venereol.* **37**, 1897–1905 (2023).
20. Chauvel-Picard, J. et al. Line-field confocal optical coherence tomography as a tool for three-dimensional in vivo quantification of healthy epidermis: A pilot study. *J. Biophoton.* **15**, e202100236 (2022).
21. Pedrazzani, M. et al. Comparison of line-field confocal optical coherence tomography images with histological sections: Validation of a new method for in vivo and non-invasive quantification of superficial dermis thickness. *Ski Res. Technol.* **26**, 398–404 (2020).
22. Breugnot, J. et al. Utilizing deep learning for dermal matrix quality assessment on in vivo line-field confocal optical coherence tomography images. *Ski Res. Technol.* **29**, e13221 (2023).
23. Ayadh, M. et al. Investigation of the link between the human skin relief and the dermal fibers network by coupling topographic analysis and LC-OCT imaging before and during folding tests. *4open* **6**, 6 (2023).
24. Bonnier, F. et al. Line-field confocal optical coherence tomography coupled with artificial intelligence algorithms to identify quantitative biomarkers of facial skin ageing. *Sci. Rep.* **13**, 13881 (2023).
25. Haydont, V., Bernard, B. A. & Fortunel, N. O. Age-related evolutions of the dermis: Clinical signs, fibroblast and extracellular matrix dynamics. *Mech. Ageing Dev.* **177**, 150–156 (2019).
26. Reilly, D. M. & Lozano, J. Skin collagen through the lifestages: Importance for skin health and beauty. *Plast. Aesthet. Res.* **8**, 2 (2021).
27. He, T., Fisher, G. J., Kim, A. J. & Quan, T. Age-related changes in dermal collagen physical properties in human skin. *PLoS ONE* **18**, e0292791 (2023).
28. Kadoya, K. et al. Fibulin-5 deposition in human skin: Decrease with ageing and ultraviolet B exposure and increase in solar elastosis. *Br. J. Dermatol.* **153**, 607–612 (2005).
29. Lentsch, G. et al. Research techniques made simple: Emerging imaging technologies for noninvasive optical biopsy of human skin. *J. Investig. Dermatol.* **142**, 1243-1252e1 (2022).
30. Cinotti, E. et al. Comparison of reflectance confocal microscopy and line-field optical coherence tomography for the identification of keratinocyte skin tumours. *Ski Res. Technol.* **29**, e13215 (2023).
31. Neerken et al. Comparison of confocal laser scanning microscopy and optical coherence tomography. 949–971 (2004). https://doi.org/10.1007/0-387-29989-0_22
32. de Rigal, J. et al. Assessment of Aging of the human skin by in vivo Ultrasonic Imaging. *J. Investig Dermatol.* **93**, 621–625 (1989).
33. Nicolescu, A. C. et al. Subepidermal low-echogenic band—its utility in clinical practice: A systematic review. *Diagnostics* **13**, 970 (2023).
34. Czajkowska, J. et al. High-frequency ultrasound in anti-aging skin therapy monitoring. *Sci. Rep.Bold"*>*13*, 17799 (2023).
35. Cinotti, E. et al. Structural skin changes in elderly people investigated by reflectance confocal microscopy. *J. Eur. Acad. Dermatol. Venereol.* **34**, 2652–2658 (2020).
36. Wurm, E. M. T. et al. In vivo assessment of chronological ageing and photoageing in forearm skin using reflectance confocal microscopy. *Br. J. Dermatol.* **167**, 270–279 (2012).
37. Koehler, M. J., König, K., Elsner, P., Bückle, R. & Kaatz, M. In vivo assessment of human skin aging by multiphoton laser scanning tomography. *Opt. Lett.* **31**, 2879–2881 (2006).
38. Kröger, M. et al. In vivo non-invasive staining-free visualization of dermal mast cells in healthy, allergy and mastocytosis humans using two-photon fluorescence lifetime imaging. *Sci. Rep.* **10**, 14930 (2020).
39. Latriglia, F. et al. Line-field confocal optical coherence tomography (LC-OCT) for skin imaging in Dermatology. *Life* **13**, 2268 (2023).
40. Hames, S. C., Ardigò, M., Soyer, H. P., Bradley, A. P. & Prow, T. W. Automated segmentation of skin strata in Reflectance Confocal Microscopy depth stacks. *PLoS ONE* **11**, e0153208 (2016).
41. Fischman, S. et al. Non-invasive scoring of cellular atypia in keratinocyte cancers in 3D LC-OCT images using deep learning. *Sci. Rep.* **12**, 481 (2022).
42. Kaur, P., Dana, K. J., Cula, G. O. & Mack, M. C. Hybrid deep learning for reflectance confocal microscopy skin images. In *23rd International Conference on Pattern Recognition (ICPR)* 1466–1471 (2016). https://doi.org/10.1109/icpr.2016.7899844
43. Robic, J. et al. Clinical validation of a computer-based approach for the quantification of the skin ageing process of women using in vivo confocal microscopy. *J. Eur. Acad. Dermatol. Venereol.* **35**, e68–e70 (2021).
44. Setchfield, K., Gorman, A., Simpson, A. H. R. W., Somekh, M. G. & Wright, A. J. Relevance and utility of the in-vivo and ex-vivo optical properties of the skin reported in the literature: A review [Invited]. *Biomed. Opt. Express* **14**, 3555–3583 (2023).
45. Lin, C. H. et al. Rapid measurement of epidermal thickness in OCT images of skin. *Sci. Rep.* **14**, 2230 (2024).
46. Pinto-Coelho, L. How Artificial Intelligence is shaping medical imaging technology: A survey of innovations and applications. *Bioengineering* **10**, 1435 (2023).
47. Khalifa, M. & Albadawy, M. AI in diagnostic imaging: Revolutionising accuracy and efficiency. *Comput. Methods Progr. Biomed. Updat* **5**, 100146 (2024).
48. Meng, D., Zhang, S., Huang, Y., Mao, K. & Han, J. D. J. Application of AI in biological age prediction. *Curr. Opin. Struct. Biol.* **85**, 102777 (2024).
49. Bortz, J. et al. Biological age estimation using circulating blood biomarkers. *Commun. Biol.* **6**, 1089 (2023).
50. Fleischer, J. G. et al. Predicting age from the transcriptome of human dermal fibroblasts. *Genome Biol.* **19**, 221 (2018).
51. Bobrov, E. et al. PhotoAgeClock: Deep learning algorithms for development of non-invasive visual biomarkers of aging. *Aging (Albany NY)* **10**, 3249–3259 (2018).
52. Park, S. et al. Facial age evaluated by artificial intelligence system, Dr.AMORE®: An objective, intuitive, and reliable new skin diagnosis technology. *J. Cosmet. Dermatol.* **23**, 1510–1512 (2024).
53. ELKarazle, K., Raman, V. & Then, P. Facial age estimation using machine learning techniques: An overview. *Big Data Cogn. Comput.* **6**, 128 (2022).
54. Cho, C. et al. Evaluation of facial skin age based on biophysical properties in vivo. *J. Cosmet. Dermatol.* **21**, 3546–3554 (2022).
55. Dias, H. C., Manco, L., Real, F. C. & Cunha, E. A blood–bone–tooth model for Age Prediction in forensic contexts. *Biology* **10**, 1312 (2021).
56. Dubois, A. et al. Line-field confocal optical coherence tomography for high-resolution noninvasive imaging of skin tumors. *J. Biomed. Opt.* **23**, 106007–106007 (2018).
57. Ogien, J., Tavernier, C., Fischman, S. & Dubois, A. Line-field confocal optical coherence tomography (LC-OCT): Principles and practical use. *Ital. J. Dermatol. Venereol.* **158**, 171–179 (2023).
58. Ogien, J., Daures, A., Cazalas, M., Perrot, J. L. & Dubois, A. Line-field confocal optical coherence tomography for three-dimensional skin imaging. *Front. Optoelectron.* **13**, 381–392 (2020).

59. Daxenberger, F. et al. Innovation in actinic keratosis assessment: Artificial Intelligence-based approach to LC-OCT PRO score evaluation. *Cancers* **15**, 4457 (2023).

Acknowledgements
COMPLIFE FRANCE for conducting the clinical study.

Author contributions
"Conceptualization: RK, FB, SR; Data Curation: FB, AA, SF, CL, MP; Formal Analysis: FB, AA, GG, SF; Funding Acquisition: RK, JHC; Investigation: FB, AA, SF; Methodology: RK, FB, SR, AA, GG, SF; Project Administration: RK, FB; Resources: RK, JHC; Supervision: RK, FB; Validation: FB, CL; Visualization: FB ; Writing - Original Draft Preparation: FB, AA, GG, RM, SF, CL; Writing - Review and Editing: FB, AA, GG, RM, AA, SR, SF, CL, MP."

Funding
The clinical study was funded by LVMH Recherche.

Declarations

Competing interests
Competing Interests Statement: SF and CL are employed by DAMAE Medical. MP is a former employee of DAMAE Medical.GG, RM, AA, SR, RK, JHC, FB are employees at LVMH Recherche. The clinical study was funded by LVMH Recherche.

Additional information
Correspondence and requests for materials should be addressed to F.B.

Reprints and permissions information is available at www.nature.com/reprints.

Publisher's note Springer Nature remains neutral with regard to jurisdictional claims in published maps and institutional affiliations.